Supplement of The Cryosphere, 20, 1–28, 2026
https://doi.org/10.5194/tc-20-1-2026-supplement

The Cryosphere Open Access EGU

Supplement of

Drivers of observed winter–spring sea-ice and snow thickness at a coastal site in East Antarctica

Diana Francis et al.

Correspondence to: Diana Francis (diana.francis@ku.ac.ae)

Supplementary Material

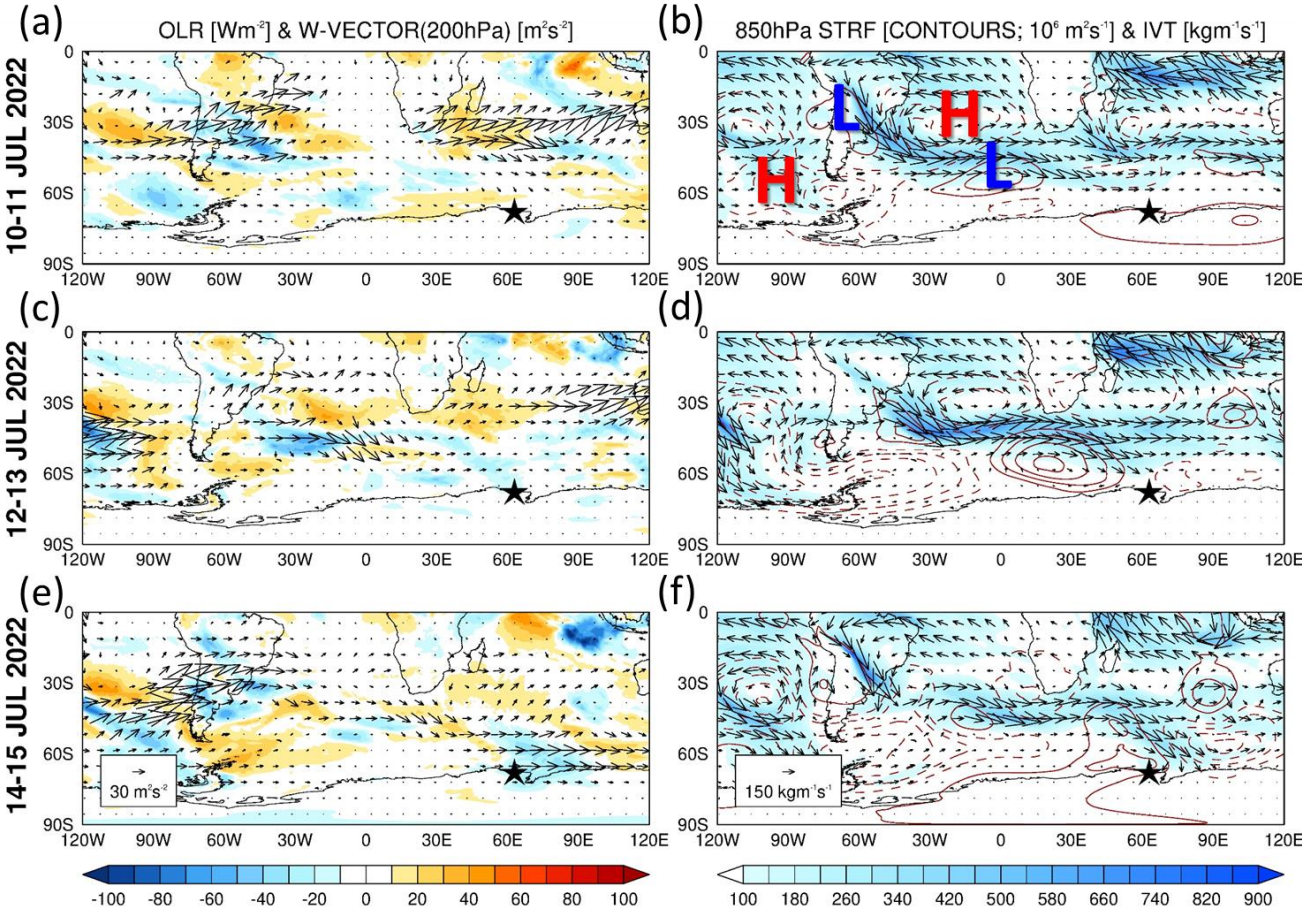

Figure S1: Atmospheric State during 10-15 July 2022: (a) Outgoing longwave radiation (OLR; shading; W m^{-2}) anomalies with respect to the 1979-2021 climatology, and stationary W vectors (Takaya and Nakamura, 2001; equations (2a) and (2b); arrows; $m^2\,s^{-2}$), and (b) 850 hPa streamfunction anomalies (contours; step of $4\times10^6\,m^2\,s^{-2}$) and integrated vapour transport (IVT; $kg\,m^{-1}\,s^{-1}$), with the shading giving the magnitude and the arrows giving the vectors, averaged over 10-11 July 2022. (c)-(d) and (e)-(f) are as (a)-(b) but averaged over 12-13 and 14-15 July 2022, respectively. The high and low pressure systems discussed in the text are highlighted in panel (b).

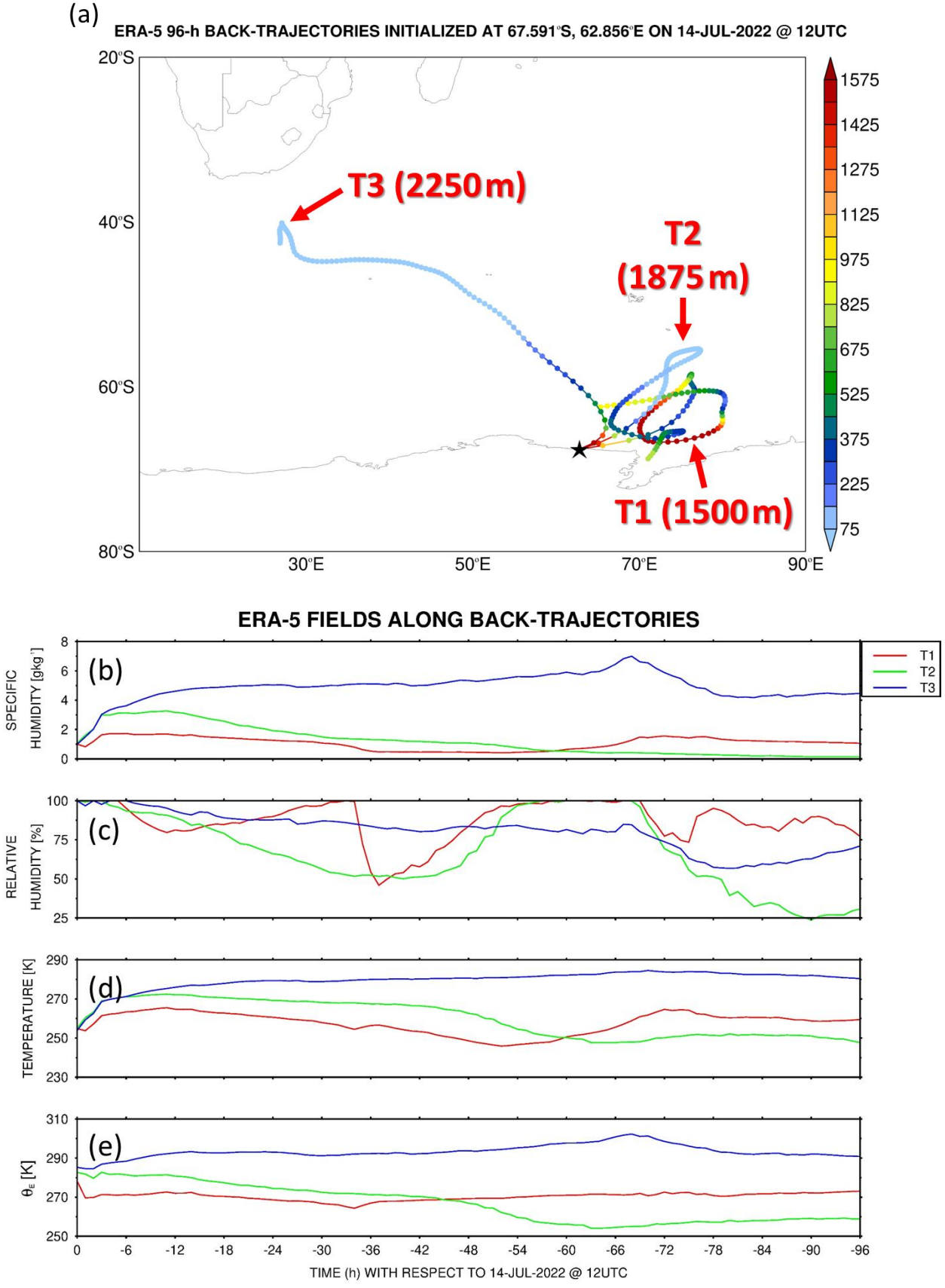
(a)
ERA-5 96-h BACK-TRAJECTORIES INITIALIZED AT 67.591°S, 62.856°E ON 14-JUL-2022 @ 12UTC
20°S
40°S
60°S
80°S
30°E
50°E
70°E
90°E
T3 (2250 m)
T2 (1875 m)
T1 (1500 m)
1575
1425
1275
1125
975
825
675
525
375
225
75
ERA-5 FIELDS ALONG BACK-TRAJECTORIES
(b)
SPECIFIC HUMIDITY [gkg-1]
T1
T2
T3
(c)
RELATIVE HUMIDITY [%]
(d)
TEMPERATURE [K]
(e)
θE [K]
TIME (h) WITH RESPECT TO 14-JUL-2022 @ 12UTC

Figure S2: Back-Trajectories initialized on 14 July 2022 at 12 UTC: (a) 96-h back-trajectories initialized at 12 UTC on 14 July 2022 at 67.591ºS, 62.856ºE and at 1500 m (T1), 1875 m (T2), and 2250 m (T3) above sea-level. The back-trajectories are obtained using the Hybrid Single-Particle Lagrangian Integrated Trajectory (HYSPLIT; Stein et al., 2015) model forced with 0.25º × 0.25º hourly ERA-5 reanalysis data. The colour of the dots gives the altitude of the parcel as it is advected backwards in time. (b)-(e) give the hourly specific humidity (g kg^{-1}), relative humidity (%), temperature (K) and equivalent potential temperature (θ_E; K), respectively, along each of the trajectories. The horizontal axis shows the time in hours backwards from the initialization time at 12 UTC on 14 July 2022.

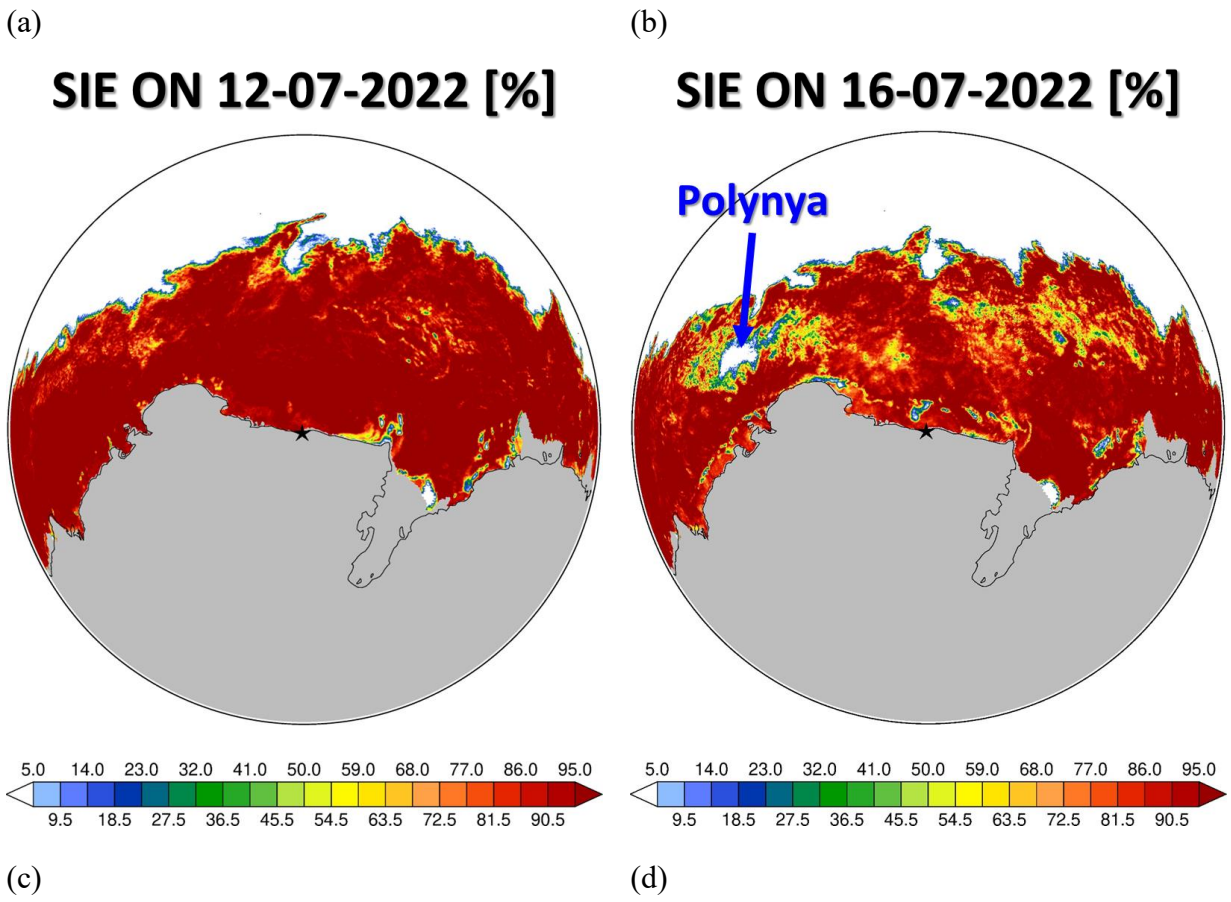

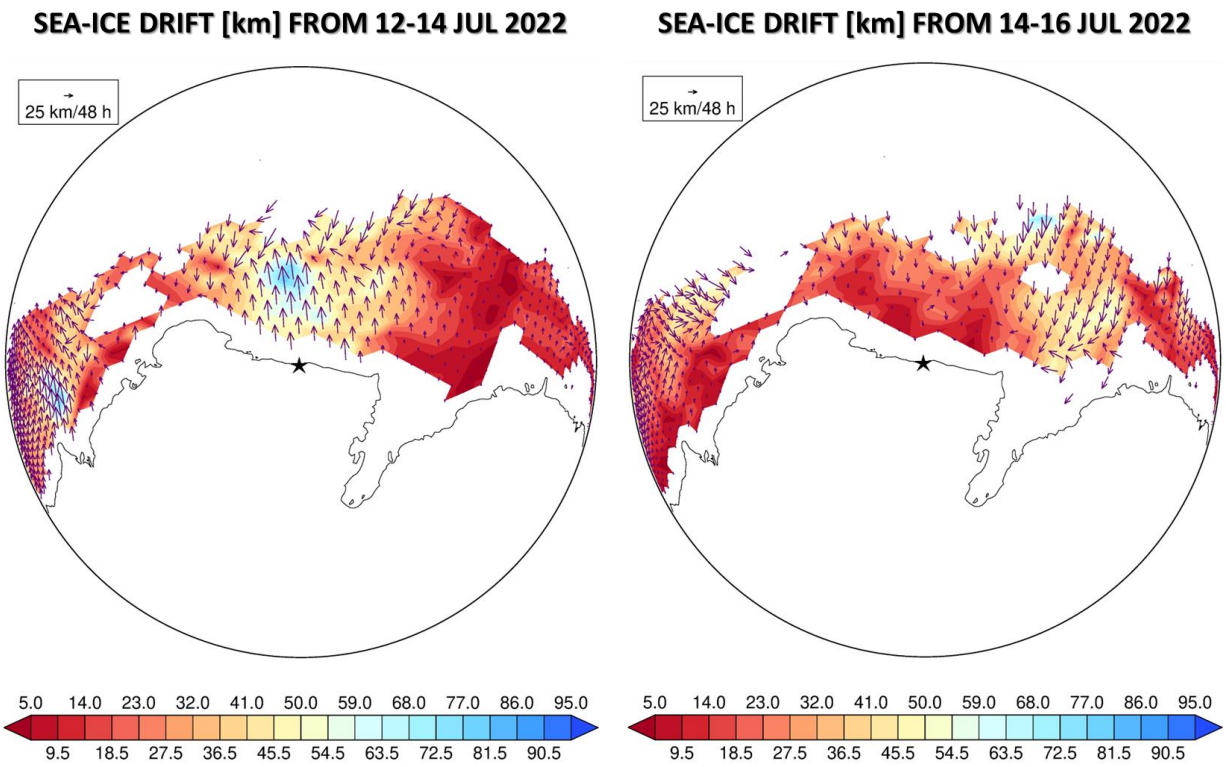

Figure S3: Effects of 14 July 2022 Atmospheric River on Sea-Ice: Sea-ice extent (SIE; %) at 3.125 km resolution around Mawson Station (star) on (a) 12 and (b) 16 July 2022. Grey shading indicates land regions. The open-ocean polynya that developed in response to the passage of the AR and attendant cyclone is highlighted in panel (b). Sea-ice velocity vectors (km 48 hr^{-1}) from a 62.5 km dataset from (c) 12 to 14 and (d) 14 to 16 July 2022, with the shading giving the magnitude. Regions for which there is no data and/or sea-ice are shaded in white.

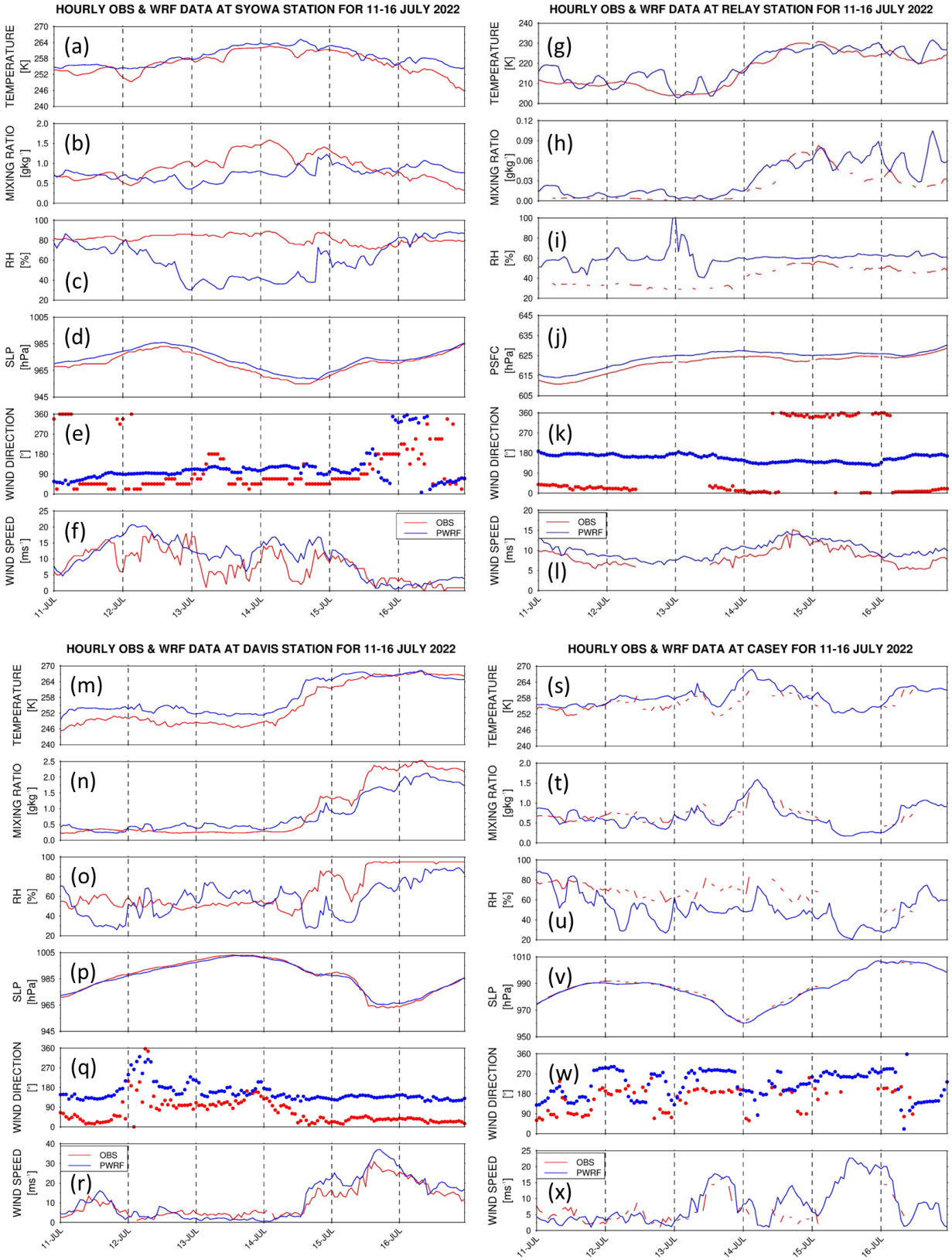

Figure S4: Evaluation of PolarWRF against Antarctica station observations: Hourly (a) air temperature (K), (b) water vapour mixing ratio (g kg^{-1}), (c) relative humidity (RH; %), (d) sea-level

pressure (SLP; hPa), and horizontal wind (e) direction (º) and (f) speed (m s^{-1}) from observations (red) and PWRF simulation (blue) for 11-16 July 2022 at the Syowa Station. (g)-(l), (m)-(r), and (s)-(x) are as (a)-(f) but at the Relay, Davis, and Casey stations in East Antarctica (Fig. 1d), respectively. For Relay Station, the surface pressure is plotted instead of the sea-level pressure in Fig. S4j.

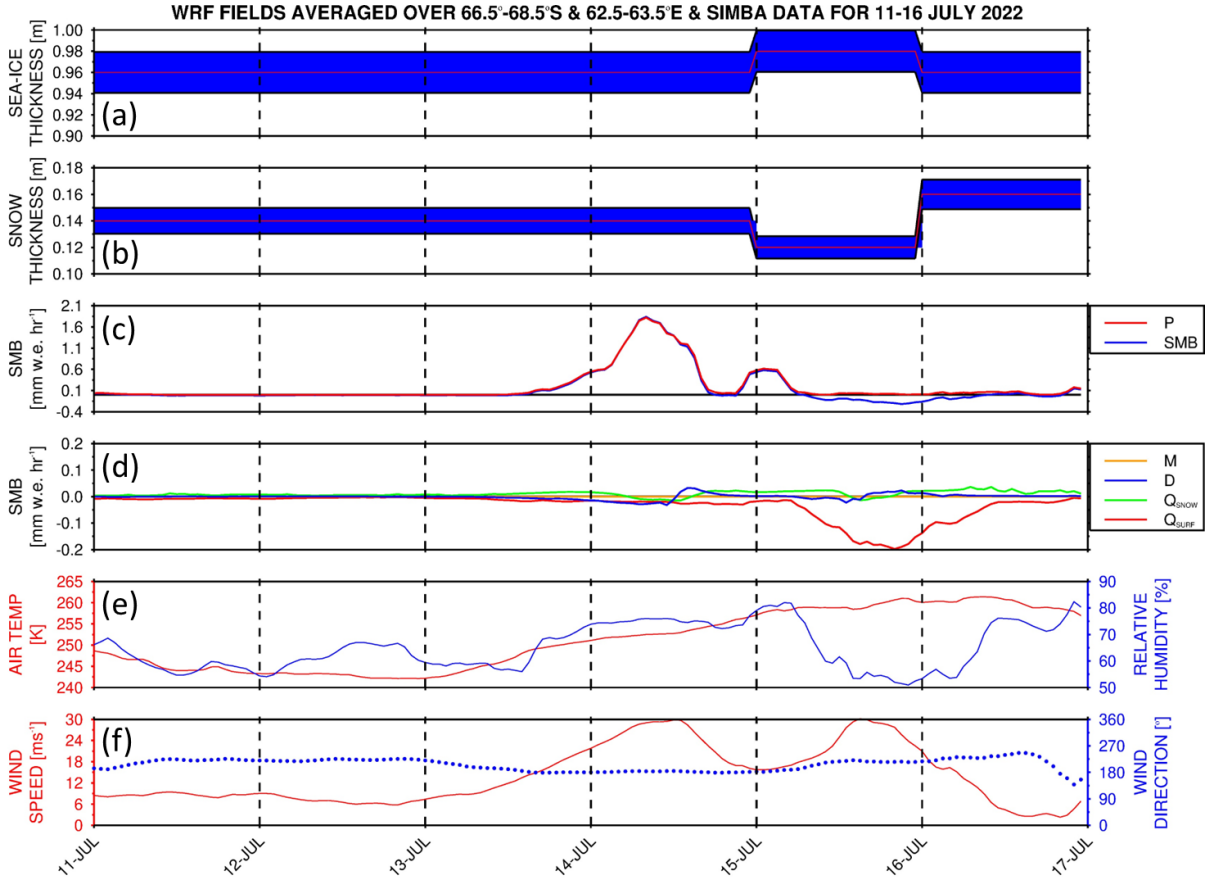

Figure S5: WRF Surface Mass Balance and SIMBA Observations: (a) ST and (b) SIT from the SIMBA measurements for the period 11-16 July 2022. The red line shows the observed values while the blue shading gives the uncertainty, which is estimated as 7% for ST and 2% for SIT (Liao et al., 2018). (c)-(d) give the hourly SMB terms (mm w.e. hr^{-1}) from WRF's 2.5 km grid averaged over the domain 66.5º-68.5ºS and 62.5º-63.5ºE. Shown is the SMB (blue) and precipitation (red; P) in (c), and the snowmelt (orange; M), surface sublimation (red; Q_{sfc}), blowing snow sublimation (green; Q_{snow}), and blowing snow divergence (blue; D) in (d). No snowmelt occurred during the measurement period. (e)-(f) give the model' domain averaged hourly air temperature (red; K) and relative humidity (blue; %) in (e), and horizontal wind speed (red; m s^{-1}) and direction (blue; º) in (f).

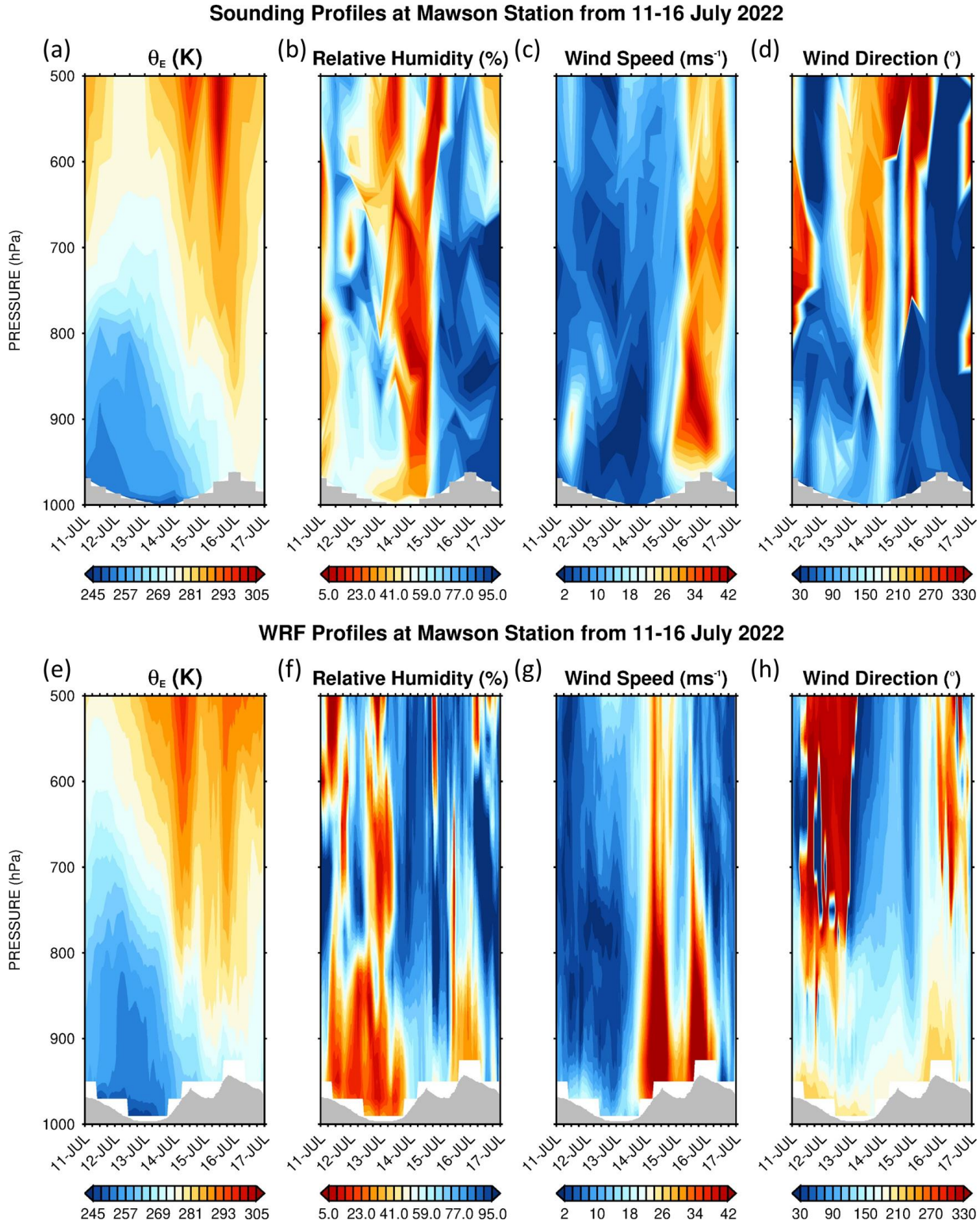
Sounding Profiles at Mawson Station from 11-16 July 2022
(a)
θE (K)
(b)
Relative Humidity (%)
(c)
Wind Speed (ms-1)
(d)
Wind Direction (°)
PRESSURE (hPa)
500
600
700
800
900
1000
11-JUL
12-JUL
13-JUL
14-JUL
15-JUL
16-JUL
17-JUL
245 257 269 281 293 305
5.0 23.0 41.0 59.0 77.0 95.0
2 10 18 26 34 42
30 90 150 210 270 330
WRF Profiles at Mawson Station from 11-16 July 2022
(e)
θE (K)
(f)
Relative Humidity (%)
(g)
Wind Speed (ms-1)
(h)
Wind Direction (°)
PRESSURE (hPa)
500
600
700
800
900
1000
11-JUL
12-JUL
13-JUL
14-JUL
15-JUL
16-JUL
17-JUL
245 257 269 281 293 305
5.0 23.0 41.0 59.0 77.0 95.0
2 10 18 26 34 42
30 90 150 210 270 330

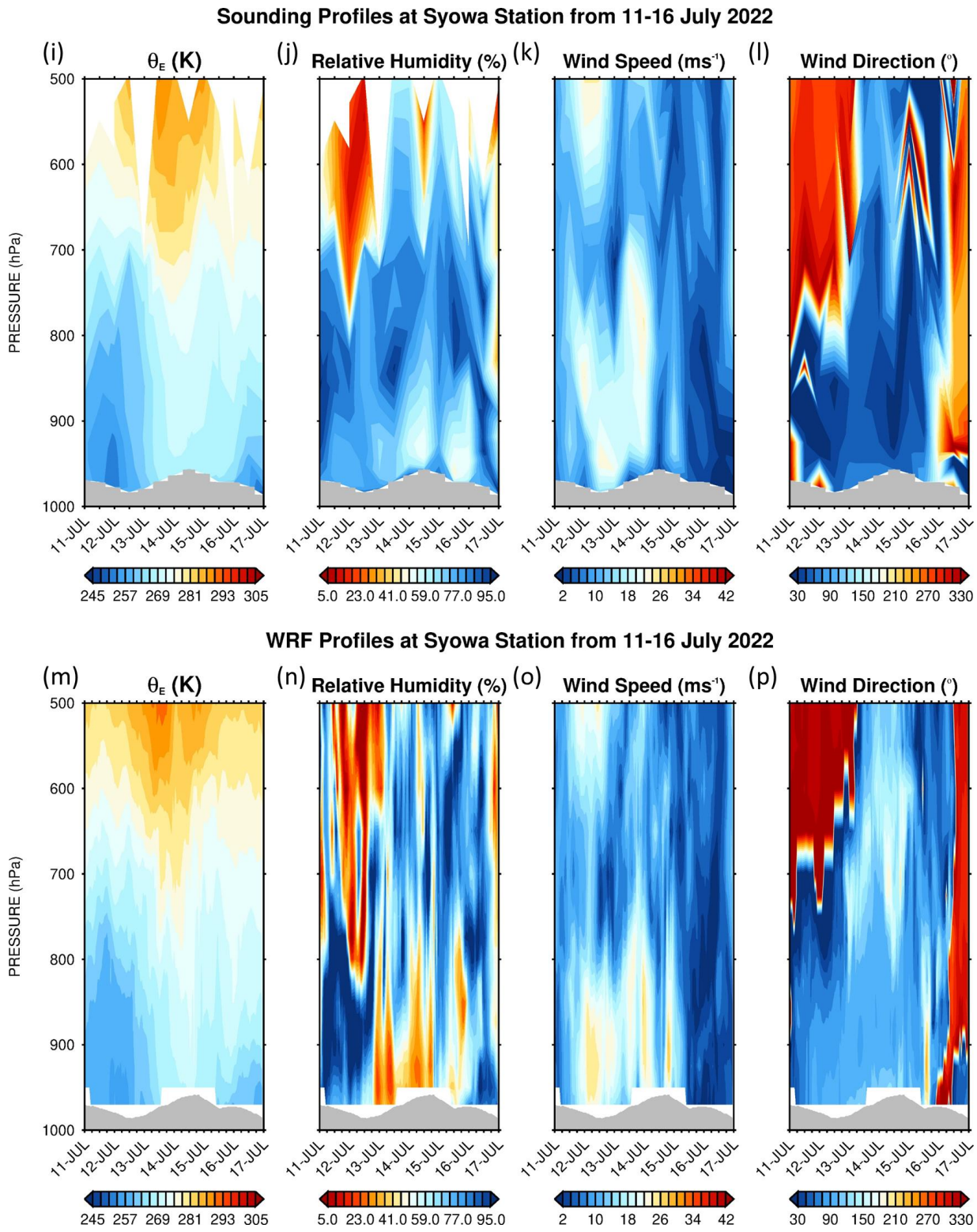

Figure S6: Evaluation of PolarWRF profiles against sounding observations at Mawson and Syowa stations: (a) Equivalent potential temperature (K), (b) relative humidity (%), and horizontal wind (c) speed (m s^{-1}) and (d) direction (º) vertical profiles at the Mawson weather station every 12 h for 11-16 July 2022 from 1000 and 500 hPa. (e)-(h) are as (a)-(d) but for the hourly profiles from PWRF simulation.

Grey shading denotes regions below topography, while white regions indicate missing data. (i)-(p) are as (a)-(h) but for the Syowa Station.

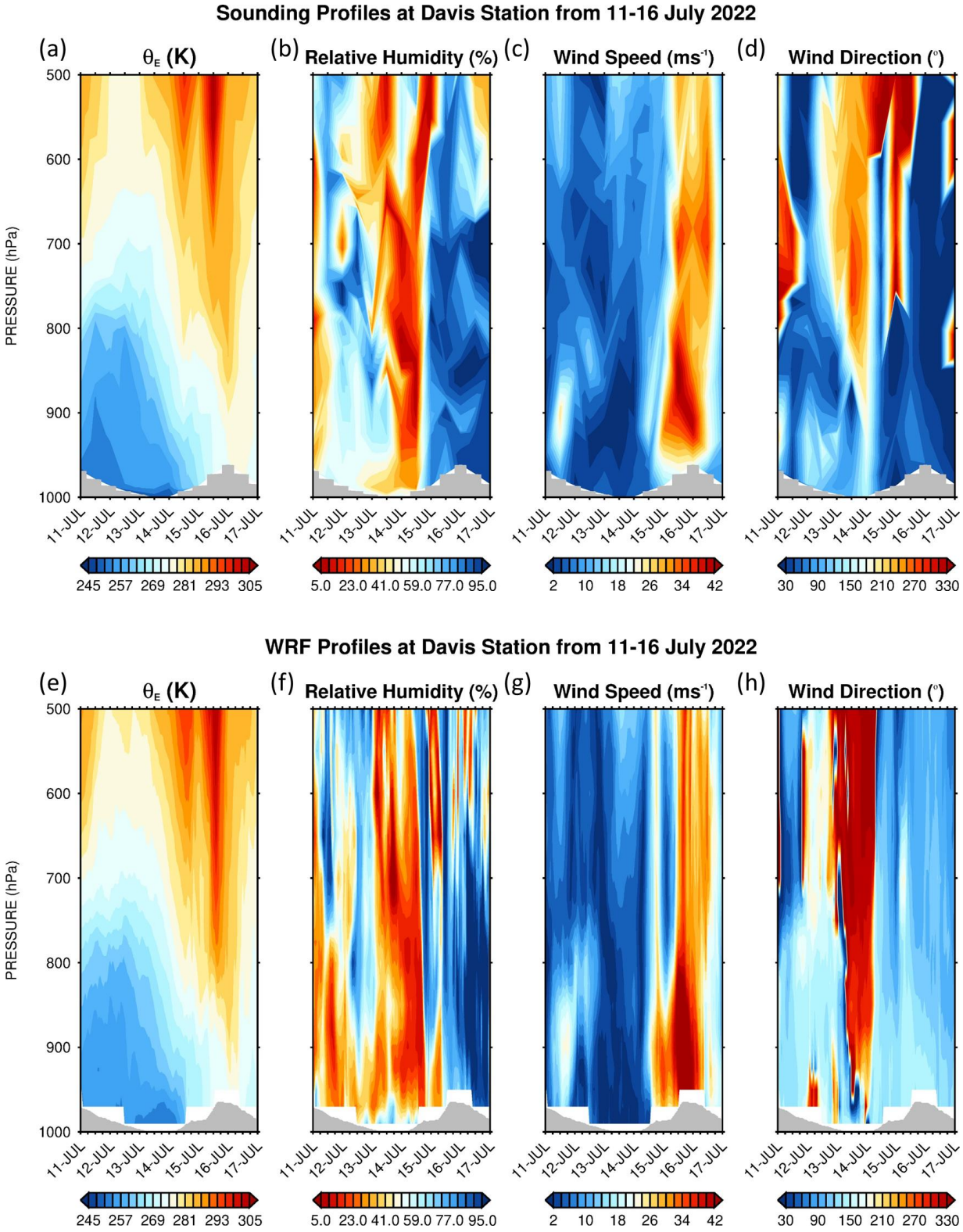

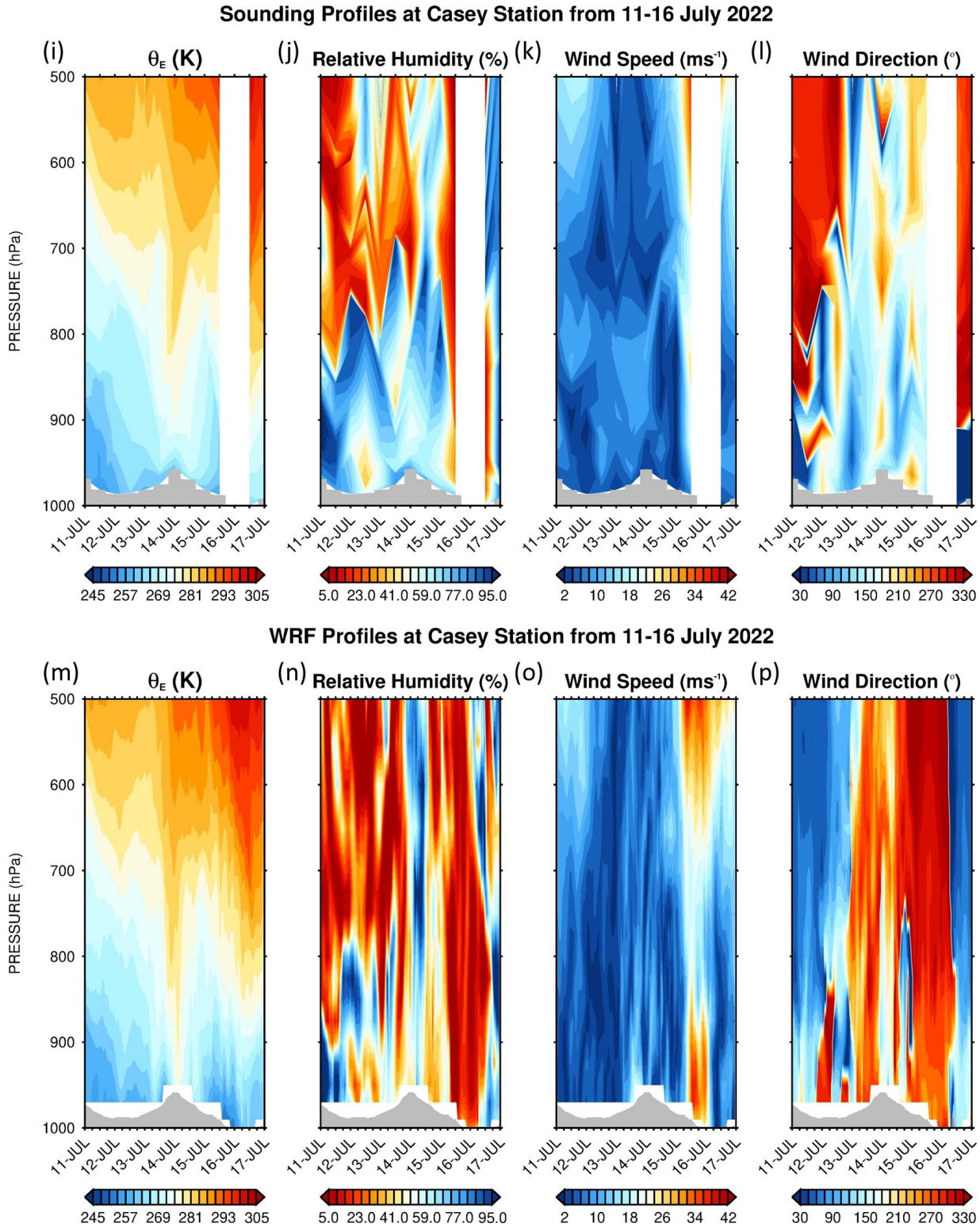

Figure S7: Evaluation of PolarWRF profiles against sounding observations at Davis and Casey stations: As Fig. S6 but for the (a)-(h) Davis and (i)-(p) Casey stations, respectively.

S.1 Verification Diagnostics

The performance of the PWRF model is assessed with the verification diagnostics defined in Equations (S1) to (S5) taken from Koh et al. (2012). They are the (i) bias, $\boldsymbol{B}$, given by the mean discrepancy between the model forecasts, F, and the observations, O; (ii) normalized bias, $\boldsymbol{\mu}$, defined as the ratio of the bias to the standard deviation of the discrepancy $\boldsymbol{B}$ between F and O. If $|\boldsymbol{\mu}| < 0.5$, the bias makes a smaller contribution to the Root Mean Square Error than the error variance and can therefore can be regarded as not significant; (iii) correlation, ρ, which measures the phase agreement between the modelled and observed data; (iv) variance similarity, η, an indication of the amplitude agreement between the two signals; and (v) normalized error variance, α, a diagnostic that combines phase and amplitude errors. For a random forecast based on the climatological mean and variance, $\alpha = 1$, and hence the model predictions can be deemed as practically useful if $\alpha < 1$. The ρ, η and α skill scores are non-dimensional, symmetrical with respect to observations and forecasts, and applicable to scalar and vector fields - meaning that the model performance for scalars such as air temperature and vector quantities such as the wind vector can be directly compared.

$$\boldsymbol{B} = \boldsymbol{F} - \boldsymbol{O} \quad (S1)$$

$$\boldsymbol{\mu} = \frac{<\boldsymbol{D}>}{\sigma_D} \quad (S2)$$

$$\rho = \frac{1}{\sigma_O \sigma_F} < (\boldsymbol{F} - <\boldsymbol{F}>) \cdot (\boldsymbol{O} - <\boldsymbol{O}>) >; \; -1 \leq \rho \leq 1 \quad (S3)$$

$$\eta = \frac{\sigma_O \sigma_F}{\frac{1}{2}(\sigma_O^2 + \sigma_F^2)}; \; 0 \leq \eta \leq 1 \quad (S4)$$

$$\alpha = 1 - \rho\eta = \frac{\sigma_D^2}{\sigma_O^2 + \sigma_F^2}; \; 0 \leq \alpha \leq 2 \quad (S5)$$

S.2 Southern Annular Mode (SAM) and the Pook Blocking Index

For ARs to reach Antarctica, a large-scale circulation pattern that favours the advection of the warm and moist low-latitude air masses into the continent must be present. The leading mode of variability in the Southern Hemisphere extratropics is the Southern Annular Mode (SAM; Marshall, 2003). This metric is based on the difference in mean sea-level pressure averaged over six stations at ~40ºS and six stations at ~65ºS, which are deemed representative of the zonal flow at the two latitudes. A positive index value indicates a stronger westerly flow in the Southern Hemisphere mid-latitudes, while a negative SAM phase is accompanied by an increase in blocking frequency (Oliveira et al., 2013). Atmospheric blocking promotes the development and propagation of ARs (Massom et al., 2004; Francis et al., 2021, 2022a; Wille et al., 2024). In this study, it is quantified using the blocking index (BI) proposed by Pook et al. (2013) and optimized over Antarctica by Wille et al. (2024c):

$$BI = 0.5\,(U_{35} + U_{40} + U_{65} + U_{70} - U_{50} - U_{60} - 2U_{55}) \quad (S6)$$

where U_X is the geostrophic zonal wind computed from the 5-day running mean (in order to exclude temporary features) of the 500 hPa geopotential height at latitude XºS. Mid-latitude blocking events correspond to a positive BI, with values in excess of 40 m s^{-1} indicating a high degree of blocking.

S.3 Tropopause Polar Vortices (TPVs)

The poleward transport of warm and moist low-latitude air is linked to the strength of the attendant cyclone, which is itself modulated by the presence of TPVs. As detailed in Wille et al. (2024c), TPVs are characterized by a minimum in potential temperature and a maximum in potential vorticity at the dynamic tropopause (PV = 2×10^{-6} m^2 K s^{-1} kg^{-1} = 2 PV Units = 2 PVU in the Northern Hemisphere and -2 PVU in the Southern Hemisphere). When co-located with increased low-level baroclinicity, they can trigger cyclogenesis, with a deeper low promoting an enhanced poleward propagation of the warm and moist low-latitude air mass. The TPVs are identified using the TPVTrack (v1.0) software described in Szapiro and Cavallo (2018), here driven by ERA-5 data.

S.4 Surface Mass Balance (SMB) Parameterization

As detailed in Francis et al. (2023), three terms of the SMB (Equation 3), are parameterized. They are the surface sublimation rate, Q_{sfc} , blowing snow sublimation rate, Q_{snow}, and blowing snow divergence D, all with units of mm w.e. hr^{-1}. Q_{sfc} is parameterized as

$$Q_{sfc} = \frac{\rho' \rho_{air}}{\rho_{water}} \left\{ \left[\frac{\kappa U}{ln\left(\frac{z+z_0}{z_0}\right)} \right] \left[\frac{\kappa\, q_{si}\,(RH_{ice}-1)}{ln\left(\frac{z+z_q}{z_q}\right)} \right] \right\} \quad (S9)$$

where κ is the von Karman constant (0.4); U is the wind speed at height z above the surface (here 10-m; m s^{-1}); z_0 is the aerodynamic roughness length (m); q_{si} is the saturation mixing ratio over ice (kg kg^{-1}); RH_{ice} is the relative humidity with respect to ice; z_q is the thermal roughness length for moisture over snow (m), taken to be the same as z_0; ρ' is a conversion factor from m s^{-1} to mm day-1 (8.64×10^7); ρ_{air} is the air density (kg m^{-3}); ρ_{water} is the density of water (1000 kg m^{-3}). As noted in Dery and Yau (2002), a positive Q_{sfc} indicates deposition and a negative Q_{sfc} indicates sublimation.

The blowing snow sublimation rate, Q_{snow}, is expressed as:

$$Q_{snow} = \left(a_0 + a_1\xi + a_2\xi^2 + a_3\xi^3 + a_4U_{10} + a_5\xi U_{10} + a_6\xi^2 U_{10} + a_7U_{10}^2 + a_8\xi U_{10}^2 + a_9U_{10}^3\right)/U' \quad (S10)$$

with $\xi = \frac{RH_{ice} - 1}{2\,\rho_{ice}\,[F_k(T) + F_d(T)]}$; $U' = \frac{\left(1 - \frac{U_t}{U_{10}}\right)^{2.59}}{\left(1 - \frac{6.975}{U_{10}}\right)^{2.59}}$; $U_t = 6.975 + 0.0033(T_{2m} + 27.27)^2$

In equation (S10), ξ is a thermodynamic term ($m^2\ s^{-1}$); ρ_{ice} is the density of ice ($917\ kg\ m^{-3}$); U_{10} is the 10-m wind speed ($m\ s^{-1}$); U' is a non-dimensional factor that removes the dependence on the saltation mixing ratio; U_t is the threshold for initiation of blowing snow ($m\ s^{-1}$); T_{2m} is the 2-m temperature (ºC); $F_k(T)$ and $F_d(T)$ are the conductivity and diffusion terms associated with sublimation ($m\ s\ kg^{-1}$). The constants a_0 to a_9 are given by 3.78407×10^{-1}, -8.64089×10^{-2}, -1.60570×10^{-2}, 7.25516×10^{-4}, -1.25650×10^{-1}, 2.48430×10^{-2}, -9.56871×10^{-4}, 1.24600×10^{-2}, 1.56862×10^{-3} and -2.93002×10^{-4}, respectively.

The blowing snow divergence D, is defined as:

$$D = \frac{\rho'}{\rho_{water}} \nabla \cdot (B\ U_{10}^{C}) \quad (S11)$$

where the constants B and C are given by $2.2 \times 10^{-6}\ kg\ m^{-5.04}\ s^{3.04}$ and 4.04, respectively.